Available online at www.sciencedirect.com

ScienceDirect

Physics Procedia 61 (2015) 658 – 665

Physics Procedia

Radon-Related Backgrounds in the LUX Dark Matter Search

A. Bradley[a], D.S. Akerib[a], H.M. Araújo[b], X. Bai[c], A.J. Bailey[b], J. Balajthy[d], E. Bernard[e], A. Bernstein[f], D. Byram[g], S.B. Cahn[e], M.C. Carmona-Benitez[h], C. Chan[i], J.J. Chapman[i], A.A. Chiller[g], C. Chiller[g], T. Coffey[a], A. Currie[b], L. de Viveiros[j], A. Dobi[d], J. Dobson[k], E. Druszkiewicz[l], B. Edwards[e], C.H. Faham[m], S. Fiorucci[i], C. Flores[n], R.J. Gaitskell[i], V.M. Gehman[m], C. Ghag[o], K.R. Gibson[a], M.G.D. Gilchriese[m], C. Hall[d], S.A. Hertel[e], M. Horn[e], D.Q. Huang[i], M. Ihm[p], R.G. Jacobsen[p], K. Kazkaz[f], R. Knoche[d], N.A. Larsen[e], C. Lee[a], A. Lindote[j], M.I. Lopes[j], D.C. Malling[i], R. Mannino[q], D.N. McKinsey[e], D.-M. Mei[g], J. Mock[n], M. Moongweluwan[l], J. Morad[n], A.St.J. Murphy[k], C. Nehrkorn[h], H. Nelson[h], F. Neves[j], R.A. Ott[n], M. Pangilinan[i], P.D. Parker[e], E.K. Pease[e], K. Pech[a], P. Phelps[a], L. Reichhart[o], T. Shutt[a], C. Silva[j], V.N. Solovov[j], P. Sorensen[f], K. O'Sullivan[e], T.J. Sumner[b], M. Szydagis[n], D. Taylor[r], B. Tennyson[e], D.R. Tiedt[c], M. Tripathi[n], S. Uvarov[n], J.R. Verbus[i], N. Walsh[n], R. Webb[q], J.T. White[q,1], M.S. Witherell[h], F.L.H. Wolfs[l], M. Woods[n], C. Zhang[d]

[a] *Case Western Reserve University, Dept. of Physics, 10900 Euclid Ave, Cleveland OH 44106, USA*
[b] *Imperial College London, High Energy Physics, Blackett Laboratory, London SW7 2BZ, UK*
[c] *South Dakota School of Mines and Technology, 501 East St Joseph St., Rapid City SD 57701, USA*
[d] *University of Maryland, Dept. of Physics, College Park MD 20742, USA*
[e] *Yale University, Dept. of Physics, 217 Prospect St., New Haven CT 06511, USA*
[f] *Lawrence Livermore National Laboratory, 7000 East Ave., Livermore CA 94551, USA*
[g] *University of South Dakota, Dept. of Physics, 414E Clark St., Vermillion SD 57069, USA*
[h] *University of California Santa Barbara, Dept. of Physics, Santa Barbara, CA, USA*
[i] *Brown University, Dept. of Physics, 182 Hope St., Providence RI 02912, USA*
[j] *LIP-Coimbra, Department of Physics, University of Coimbra, Rua Larga, 3004-516 Coimbra, Portugal*
[k] *SUPA, School of Physics and Astronomy, University of Edinburgh, Edinburgh, EH9 3JZ, UK*
[l] *University of Rochester, Dept. of Physics and Astronomy, Rochester NY 14627, USA*
[m] *Lawrence Berkeley National Laboratory, 1 Cyclotron Rd., Berkeley, CA 94720, USA*
[n] *University of California Davis, Dept. of Physics, One Shields Ave., Davis CA 95616, USA*
[o] *Department of Physics and Astronomy, University College London, Gower Street, London WC1E 6BT, UK*
[p] *University of California Berkeley, Department of Physics, Berkeley, CA 94720, USA*
[q] *Texas A & M University, Dept. of Physics, College Station TX 77843, USA*
[r] *South Dakota Science and Technology Authority, Sanford Underground Research Facility, Lead, SD 57754, USA*

Email address: awbradley@case.edu (A. Bradley)

[1] deceased

Selection and peer review is the responsibility of the Conference lead organizers, Frank Avignone, University of South Carolina, and Wick Haxton, University of California, Berkeley, and Lawrence Berkeley Laboratory

doi:10.1016/j.phpro.2014.12.067

Abstract

The LUX detector is currently in operation at the Davis Campus at the 4850' level of the Sanford Underground Research Facility (SURF) in Lead, SD to directly search for WIMP dark matter. Knowing the type and rate of backgrounds is critical in a rare, low energy event search, and LUX was designed, constructed, and deployed to mitigate backgrounds, both internal and external. An important internal background are decays of radon and its daughters. These consist of alpha decays, which are easily tagged and are a tracer of certain backgrounds, and beta decays, some of which are not as readily tagged and present a background for the WIMP search. We report on studies of alpha decay and discuss implications for the WIMP search.

Selection and peer review is the responsibility of the Conference lead organizers, Frank Avignone, University of South Carolina, and Wick Haxton, University of California, Berkeley, and Lawrence Berkeley Laboratory

Keywords: dark matter, liquid noble detectors, xenon, radon, background characterization

1. LUX Experiment and Detector

The LUX experiment is a direct search for weakly interacting massive particles (WIMPs), which could make up the dark matter [1]. The detector uses a total of 370 kg of liquefied xenon (LXe) with 250 kg actively instrumented as a time projection chamber (TPC). It is deployed at the 4850' Level of the Sanford Underground Research Facility (SURF) in Lead, SD [2]. The first WIMP search results from LUX are reported in [3]. Background characterization and mitigation is very important for low-energy rare event searches like LUX [4]. To limit the backgrounds the detector is constructed from materials screened for radioactivity, is deployed underground to shield against cosmic radiation, and uses a water tank to shield out neutrons and gammas from the rock walls. This work used 3.8 live days of data collected with no calibration sources present between May and June 2013 to investigate events from the alpha decays in the ^{238}U and ^{232}Th decay chains. Here we report on the alpha event rates and energy spectrum, and discuss the related WIMP search backgrounds.

The LUX TPC, depicted in fig. 1, has two 61-channel PMT arrays above and below 270 kg LXe surrounded by a dodecagon of PTFE panels to reflect and direct primary scintillation signals (S1) to the arrays. Five electrode grids establish a 181-V/cm field to drift electrons from event sites in the LXe to a gaseous xenon (GXe) region with a 6.0-kV/cm electric field where electroluminescence produces a secondary scintillation signal (S2). This S2 light is used to determine the (x, y) position of events and the time difference of the S1 and S2 signals gives the z depth (see axes in fig. 1).

2. Event Selection and Correction

The LUX TPC aims to measure $\leq 25\,\mathrm{keV_{nr}}$ WIMP-like nuclear recoils in its active region. Alpha events with 5-9 MeV energies produce large signals and so present unique challenges. To reduce selection bias of requiring an S2 signal for alphas, the top-bottom asymmetry is used as an alternative to the S1-S2 timing between paired pulses. The top-bottom asymmetry (*TBA*), defined as $TBA = (t - b)/(t + b)$, is the difference of the light read out of the top t and bottom b PMT arrays divided by the total light read out by both arrays and correlates to z-position. Figure 2 shows the uncorrected S1 pulse area as a function of the *TBA* (left plots) and depth from the gate grid (right plots) for six apparent populations of alpha events. Events with a large z are more negative in *TBA* in fig. 2 and exhibit saturation as the light from those events are distributed among a smaller number of PMTS in the bottom array than those higher in the detector. The overall slope of the alpha signals in the top plots of fig. 2 is due to the z-dependent light collection efficiency in the bottom PMT array. We use the red-highlighted band of alpha events to derive a position-dependent correction to the S1 signals.

To properly correlate the onset of saturation in *TBA* to the event depth, the spectrum of alpha S1 signals in *TBA* is compared with the z-based spectrum of S1-S2 paried pulses. This latter spectrum is varied by varying z until the integrated counts of the largest peak in both spectra were equal. This correlates -0.7 in *TBA* to $z = 34.4$ cm. Thus data from the upper 34.4 cm of the active region are used to identify events and

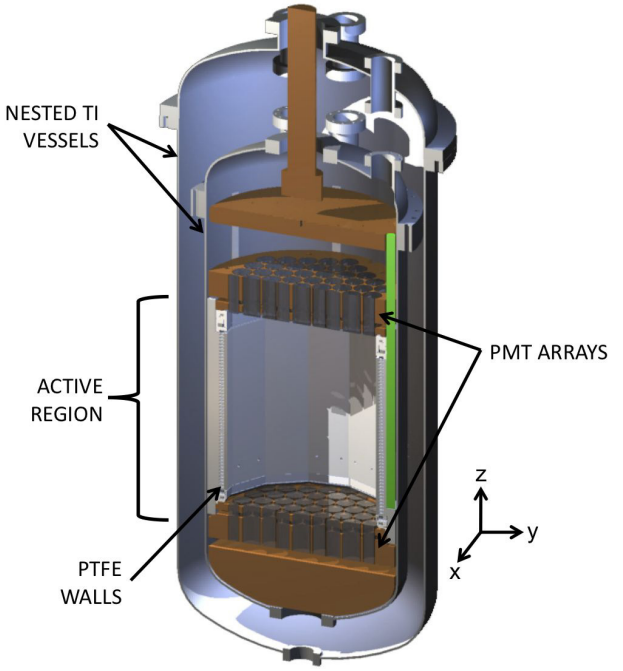

Fig. 1: Cutaway drawing of the LUX detector showing the active region, PTFE walls, PMT arrays, and nested Ti cans.

measure the event rates of the alpha populations, and these values are scaled to the full PMT-to-PMT height to account for what the 270-kg S1-sensitive region should be able to observe.

3. Energy Identification and Decay Rates

The spectrum of unpaired S1 pulses in *TBA* is scaled from pulse size in photoelectrons (phe) to energy in MeV with a single parameter scaling using the largest alpha peak (^{222}Rn) as an anchor. The alpha populations in the energy spectrum, fig. 3, are identified from the known energies of two well-known high-A decay chains: ^{238}U and ^{232}Th, which are given in table 1. The six peaks observed in the energy spectrum are fit with a sum of five Gaussians and a Crystal Ball Distribution [5] to find their individual counts, and their rates are scaled from the fractional volume to the full 270-kg PMT-to-PMT LXe volume. The results are shown in table 2. The inset in fig. 3 shows that ^{210}Po events suffer S2 loss from its location at the detector boundaries, motivating this S1-only analysis.

There are eight important alpha populations in the two decay chains, but only seven are observed in LUX, and two of the seven are indistinguishable. The ^{214}Po decay rate is suppressed due to pulse identification inefficiencies, and the rate shown here accounts for this effect. The locations of the seven alpha populations correlate to their positions in the decay chains and their respective half-lives and help explain their presence in the LUX low-background data.

4. ^{238}U and ^{232}Th Decay Chains and Alpha Locations

The locations of the alpha-emitting isotopes of the ^{238}U and ^{232}Th decay chains are shown in (r^2, z) in fig. 4a and in (x, y) in fig. 4b, with their Q-values and half-lives given in tables 1 and 2, respectively. Note that ^{210}Po, the only alpha emitter after the long-lived ^{210}Pb in the ^{238}U chain, is predominantly found on the walls and cathode, as expected due to plate-out effects. The ^{210}Po alpha decays on the PTFE reflectors are

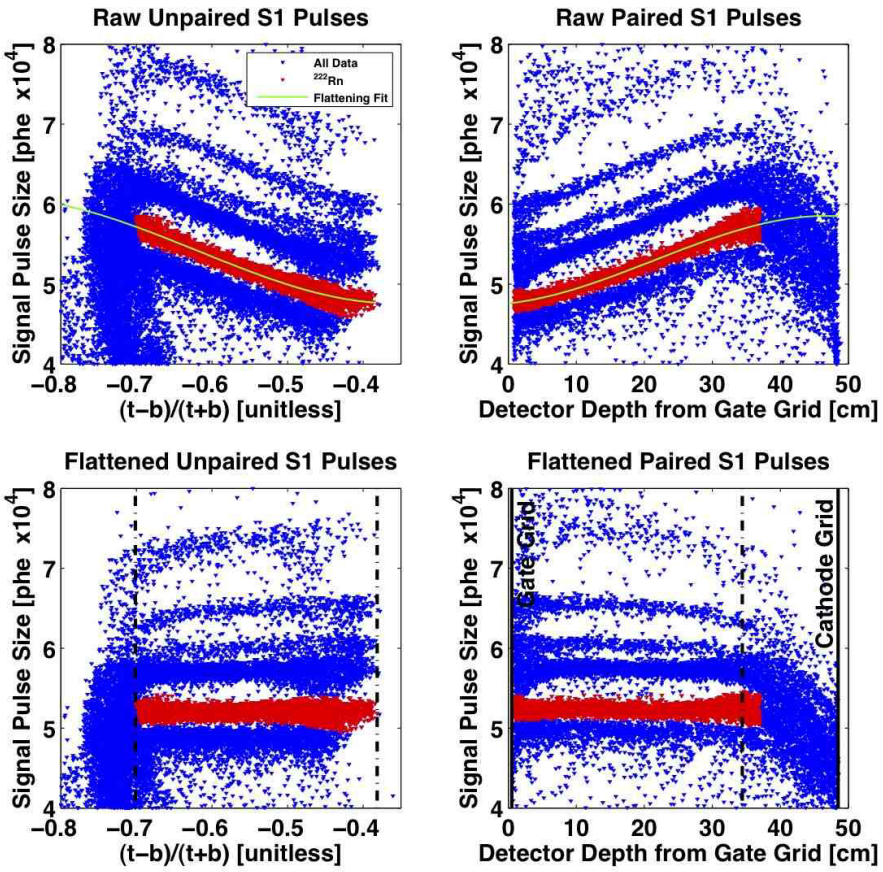

Fig. 2: (Top) Uncorrected alpha data and (bottom) alpha data corrected with the strong second band (red). The vertical dashed lines in the bottom plots enclose equal amounts of red data.

Decay Chain	Isotope	Known Energy (MeV)	Measured Energy (MeV)
^{238}U	^{222}Rn	5.59	5.59 ± 0.08*
	^{218}Po	6.16	6.12 ± 0.10
	^{214}Po	7.84	7.80 ± 0.20
	^{210}Po	5.30	5.22 ± 0.09
^{232}Th	^{220}Rn	6.41	6.47 ± 0.09
	^{216}Po	6.91	6.95 ± 0.10
	^{212}Bi	6.21	6.12 ± 0.10
	^{212}Po	8.83	not measured

Table 1: Run03 alphas found in the LUX detector, their measured energies, and their parent decay chain. Stated errors in the measured energies are the sigmas of the five Gaussian plus one Crystal Ball Distribution fit. The known energies are the decay Q-values, except for ^{210}Po, whose listed energy is the alpha energy alone because its ^{206}Pb daughter recoils into passive material (cathode, anode, or teflon). ^{218}Po and ^{212}Bi are close in energy such that they do not appear as separate peaks in the spectrum. *The ^{222}Rn line was used to anchor the S1 pulse size-to-energy scaling.

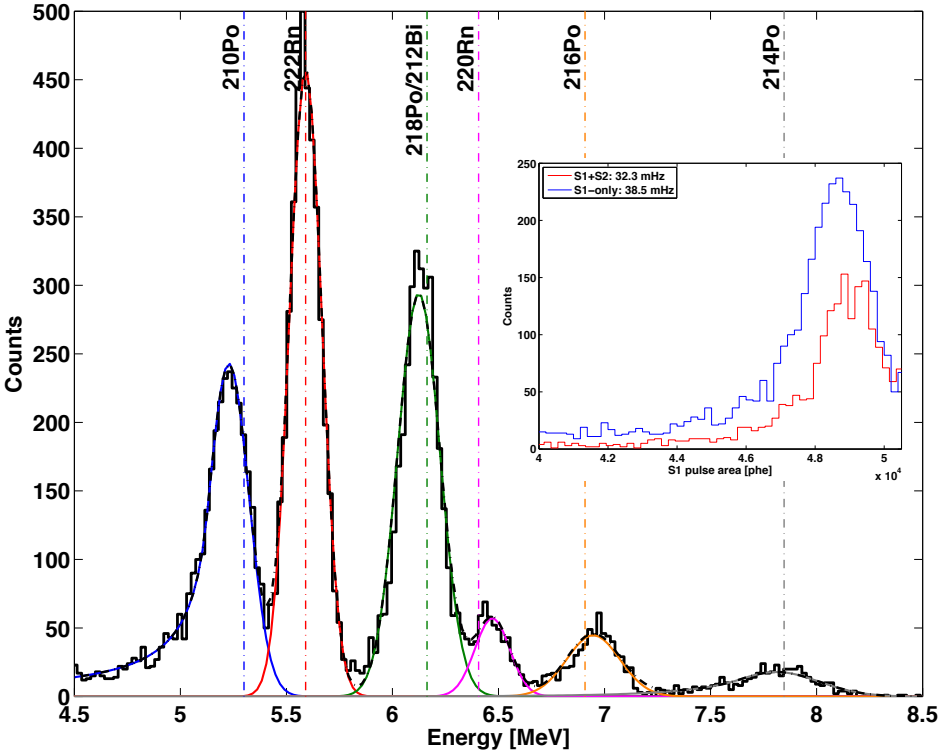

Fig. 3: Energy spectrum with fits and known energies. All vertical line energies are the decay Q-value, except for ^{210}Po, which is the alpha emission energy alone. See text regarding this apparent offset. Inset: ^{210}Po alpha event spectra of S1-only data compared to S1 pulses successfully paired with S2 pulses. The S1-S2 paired events appear at lower S1 pulse area do to energy lost in passive material from the recoiling ^{206}Pb.

potentially problematic for the dark matter search, because of the substantial (α,n) cross-section of fluorine. In LUX, however, this background source is expected to be sub-dominant (see table 3).

With their relatively short half-lives, the presence of the ^{220}Rn and ^{216}Po isotopes from the ^{232}Th chain in the first (x, y) quadrant (Q1) of the active region near the LXe surface is consistent with a source in the circulation system. This expectation is borne out by internally injected ^{83m}Kr with $t_{1/2} = 1.83$ hr, which is used for energy calibrations and circulation diagnostics of the detector. Figure 5 is a still from a movie made from a typical injection of ^{83m}Kr and shows the distribution of events throughout the LUX TPC active region 9.45 minutes from the start of the injection. Both the ^{83m}Kr events observed before they diffuse throughout the active region and the short-lived ^{220}Rn and ^{216}Po alpha events appear at the top of the active region in Q1. As the ^{83m}Kr is introduced into the active region by the circulating LXe, we infer that the ^{232}Th daughters are introduced in the same fashion. Further work is being carried out to verify this conclusion and remove this source if practical and necessary.

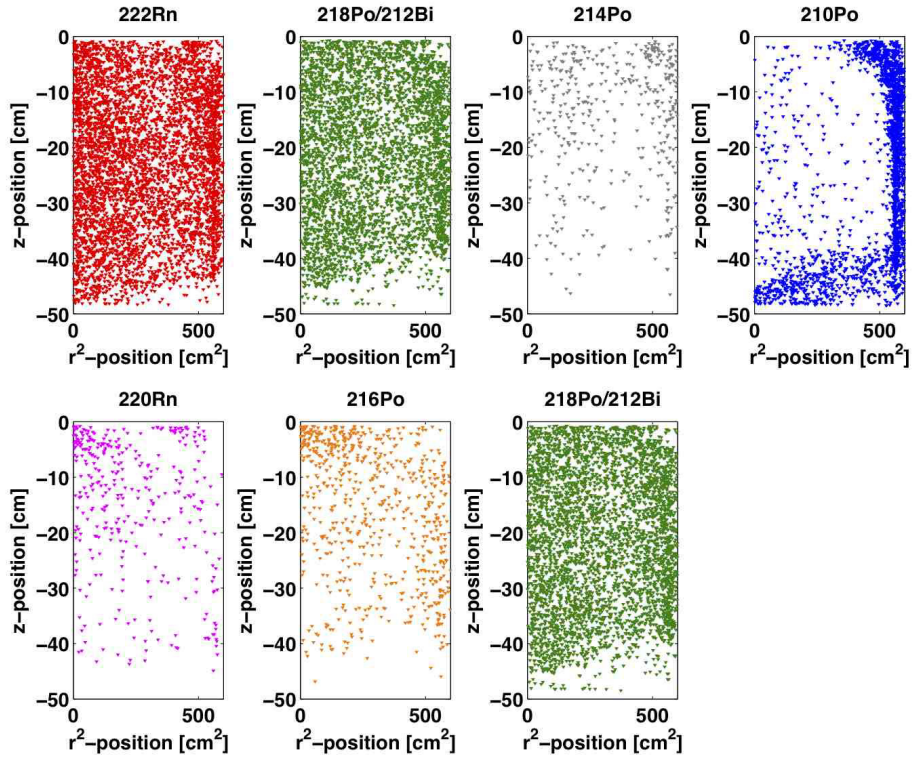

(a)

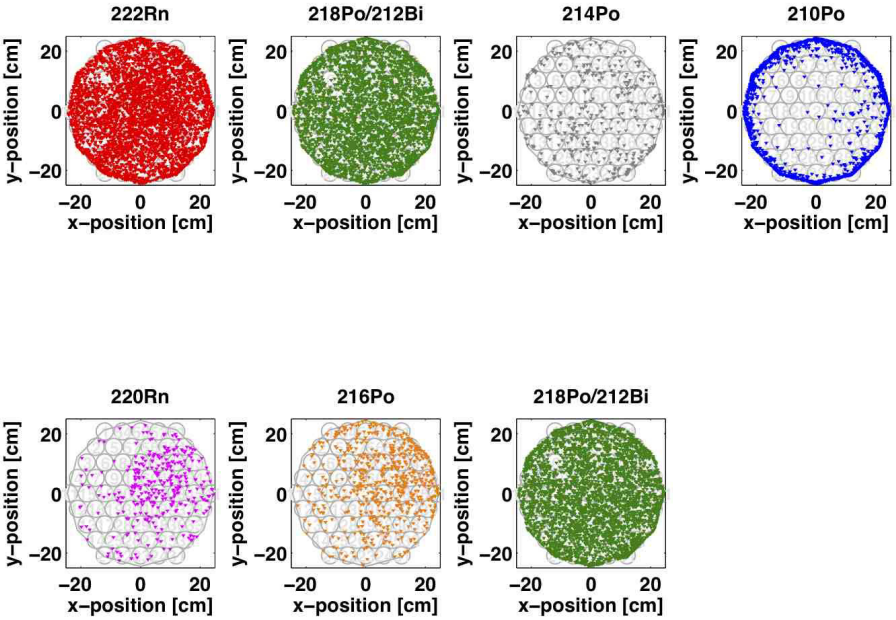

(b)

Fig. 4: The (r^2, z) (a) and (x, y) (b) locations of the alpha populations during the first WIMP data collection are explained by their half-lives and position within the respective decay chains. A dead PMT can be seen as the hole in the (x, y) distributions.

Decay Chain	Isotope	Half-life	Event Rate (mHz)	Location
^{238}U	^{222}Rn	3.82 dy	$17.9 \pm 0.2_{stat} \pm 1.3_{sys}$	Uniform in bulk
	^{218}Po	3.05 min	$14.4 \pm 0.2_{stat} \pm 1.1_{sys}$*	Uniform in bulk
	^{214}Po	162.30 μs	$3.5 \pm 0.1_{stat} \pm 0.3_{sys}$	Sparse throughout bulk
	^{210}Po	138.38 dy	> 14.3 > 7.2	Walls Cathode
^{232}Th	^{220}Rn	55.80 sec	$2.6 \pm 0.1_{stat} \pm 0.4_{sys}$	Quadrant I, sparse in bulk
	^{216}Po	0.15 sec	$2.8 \pm 0.1_{stat} \pm 0.5_{sys}$	Quadrant I, sparse in bulk
	^{212}Bi	60.54 min	$14.4 \pm 0.2_{stat} \pm 1.1_{sys}$*	Uniform in bulk
	^{212}Po	0.30 μs	not measured	not observed

Table 2: Rates of the alphas measured in the Run03 data. Statistical errors are based on $\sqrt{N}$ counting statistics. Systematic errors are from the wandering of means of the alpha energies throughout the data used in this work. The ^{214}Po rate is adjusted for a 52% event reconstruction efficiency from the measurement to the listed value. The ^{210}Po populations are suppressed due to S2 loss from their positions in the detector. *The ^{212}Bi population is undifferentiated from ^{218}Po rate, and so is reported with the same rate.

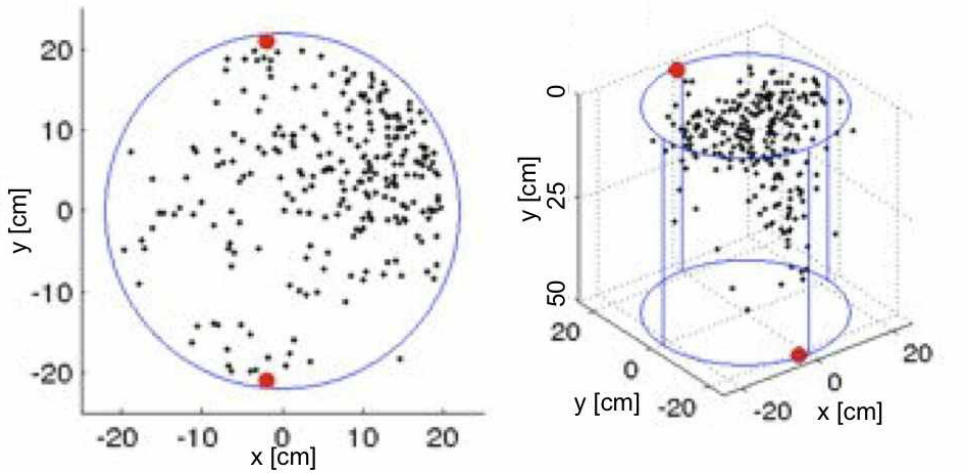

Fig. 5: A still from a movie produced during the injection of the ^{83m}Kr internal calibration source, taken 9.45 minutes after the start of the injection. The event pattern here is similar to that observed of the ^{220}Rn and ^{216}Po events, and suggests a close source of these short-lived isotopes.

5. Conclusions

The WIMP search backgrounds resulting from radon decays in LUX are listed in table 3. The F(α,n)Na rate of ^{210}Po events on the PTFE walls is subdominant to neutrons from all 122 PMTs by a factor of 33. The ^{206}Pb recoils are a nuclear recoil background, but except for possible misconstructed positions are outside the fiducial volume and so were not a large threat to the first LUX WIMP search results. The 0.10-0.41 mDRU$_{ee}$ ^{214}Pb untagged beta rate inferred from alpha decays bracketing this decay is a factor of a few lower than the PMT ER background in the detector, which mitigates the potential threat of that background [6, 7]. A gamma search in the 300-350 keV$_{ee}$ range gives a 0.23 mDRU$_{ee}$ upper bound on the ^{214}Pb beta [8]. Any backgrounds resulting from the fast ^{232}Th daughters are not expected to impact future WIMP searches and have no impact on the LUX WIMP search result reported in [3]. These background measurements were used in the overall LUX background model [8, 4] to calculate the WIMP limit published in Ref. [3].

Background	Rate	Comparison/Context
F(α,n)Na from ^{210}Po α on PTFE	14.3 mHz = 0.012 n/day	PMTs: 0.4 n/day all tubes
^{206}Pb 102 keV recoils	21.5 mHz	Fiducialization removes these
$\Gamma_{^{218}\mathrm{Po}_\alpha} > \Gamma_{^{214}\mathrm{Pb}_\beta} > \Gamma_{^{214}\mathrm{Po}_\alpha}$ ^{214}Pb untagged β 270 kg total active region	0.10-0.41 mDRU$_{ee}$ from this work $\leq$ 0.23 mDRU$_{ee}$ high-energy γ search	PMT ER BG: 0.5 mDRU$_{ee}$ in a 100 kg fiducial

Table 3: Rates of radon-related backgrounds and their comparison to other backgrounds in LUX.

References

[1] D. Akerib, et al., The Large Underground Xenon (LUX) Experiment, Nucl.Instrum.Meth. A704 (2013) 111–126. arXiv:1211.3788, doi:10.1016/j.nima.2012.11.135.

[2] D. Akerib, et al., Technical Results from the Surface Run of the LUX Dark Matter Experiment, Astropart.Phys. 45 (2013) 34–43. arXiv:1210.4569, doi:10.1016/j.astropartphys.2013.02.001.

[3] D. Akerib, et al., First results from the lux dark matter experiment at the sanford underground research facility, Phys. Rev. Lett. 112 (2014) 091303. doi:10.1103/PhysRevLett.112.091303.

[4] D. Akerib, et al., Radiogenic and Muon-Induced Backgrounds in the LUX Dark Matter Detector, , Astropart.Phys.arXiv:1403.1299.

[5] J. E. Gaiser, Charmonium Spectroscopy from Radioactive Decays of the J/ψ and ψ', Ph.D. thesis, Stanford University (August 1982).

[6] D. Malling, The LUX Experiment - Background Model and Physics Goals, APS April Meeting, Denver, CO, 2013-04-13 (2013).

[7] A. W. Bradley, LUX Thermosyphon Cryogenics and Radon-Related Background for the First WIMP Result, Ph.D. thesis, Case Western Reserve University (May 2014).

[8] D. Malling, Measurement and Analysis of WIMP Detection Backgrounds, and Characterization and Performance of the Large Underground Xenon Dark Matter Search Experiment, Ph.D. thesis, Brown University (May 2014).